Topological susceptibility and string tension in the lattice CP^{N-1} models

Massimo Campostrini, Paolo Rossi, and Ettore Vicari
Dipartimento di Fisica dell'Università and Istituto Nazionale di Fisica Nucleare, I-56126 Pisa, Italy
(Received 3 August 1992)

In the lattice CP^{N-1} models we study the problems related to the measure of observables closely connected to the dynamically generated gauge field, such as the topological susceptibility and the string tension. We perform numerical simulations at $N = 4$ and $N = 10$. In order to test the universality, we adopt two different lattice formulations. Scaling and universality tests lead to the conclusion that at $N = 10$ the geometrical approach gives a good definition of lattice topological susceptibility. On the other hand, $N = 4$ proves not to be large enough to suppress the unphysical configurations, called dislocations, contributing to χ_t^g (at least up to $\xi \simeq 30$ in our lattice formulations). We obtain other determinations of χ_t by the field-theoretical method, which relies on a local definition of the lattice topological charge density, and the cooling method. They give quite consistent results, showing scaling and universality. The large-N expansion predicts an exponential area law behavior for sufficiently large Wilson loops, which implies confinement, due to the dynamical matter fields and absence of the screening phenomenon. We determine the string tension, without finding evidence of screening effects.

PACS number(s): 11.15.Ha, 11.15.Pg, 75.10.Hk

I. INTRODUCTION

Two-dimensional CP^{N-1} models play an important role as a theoretical laboratory for testing nonperturbative analytical and numerical methods in a confining, asymptotically free quantum field theory. A pleasant feature of these models is the possibility of performing a systematic $1/N$ expansion around the large-N saddle-point solution. Indeed, most properties of CP^{N-1} models have been obtained in the context of the $1/N$ expansion [1–3].

An alternative and more general nonperturbative approach is the simulation of the theory on the lattice. Recently there has been considerable interest in simulations of lattice CP^{N-1} models [4–11].

The purpose of the present paper is that of presenting rather complete numerical results concerning the CP^3 and the CP^9 models. We especially analyze the problems related to the measure of observables closely connected to the dynamical gauge field, such as the topological susceptibility and the string tension.

A troublesome point in the lattice simulation technique is the study of the topological properties. Measuring the topological susceptibility χ_t from discrete configurations proves to be a nontrivial task.

It is well known that, in the two-dimensional (2D) O(3) σ model or CP^1 model, geometrical definitions of topological charge are plagued by the presence of dislocations [12, 13], i.e., topological structures of the size of one lattice spacing, whose unphysical contribution to χ_t does not vanish in the continuum limit. As a consequence, the topological susceptibility derived from these definitions does not show the expected scaling behavior.

The general belief is that for higher values of N the above problems should disappear. But the situation for the CP^3 model appears still problematic. There have been recent attempts [5, 7, 8, 10] to determine χ_t by using the geometrical method, but the results are not consistent. The authors of Refs. [8] and [10] both claim to observe scaling but they find different values for χ_t (about a factor 2 of difference). Since they use two different lattice formulations, the geometrical measure would violate universality. Furthermore, the authors of Ref. [7], using the same lattice formulation as in Ref. [10], do not even see scaling.

An alternative approach relies on a definition of the topological charge density by a local polynomial in the lattice variables. Local operator definitions are not affected by the dislocation problem but unavoidably lead to mixing with lower and equal dimension operators and to the need of subtracting perturbative tails and performing finite renormalizations [14]. Neverthless, this method allowed for the determination of the topological susceptibility of the CP^1 or O(3) σ model [4, 14].

Another important property of the CP^{N-1} models is the appearance of a linear confining potential between non-gauge-invariant states. The large-N expansion predicts an exponential area law behavior for sufficiently large Wilson loops. The persistence of the area law at large distance would imply the absence of the screening phenomenon due to the dynamical "matter fields." The point we wish to clarify is whether at finite N the screening phenomenon is recovered, or the large-N prediction is confirmed.

This paper is organized as follows.

In Sec. II the lattice actions adopted for numerical simulations are presented and the lattice definitions of physical observables are introduced.

In Sec. III we discuss specific features of the simulations of the CP^3 and CP^9 models, and present the corre-

sponding numerical results.

In Sec. IV problems related to the evaluation of the topological susceptibility are carefully analyzed.

In Sec. V we discuss the determination of the string tension from the Wilson loops.

II. LATTICE FORMULATION

We choose to regularize the theory on the lattice by considering the action:

$$S_g = -N\beta \sum_{n,\mu} (\bar{z}_{n+\mu} z_n \lambda_{n,\mu} + \bar{z}_n z_{n+\mu} \bar{\lambda}_{n,\mu} - 2), \quad (1)$$

where z_n is an N-component complex scalar field, constrained by the condition

$$\bar{z}_n z_n = 1 \quad (2a)$$

and $\lambda_{n,\mu}$ is a U(1) gauge field satisfying

$$\bar{\lambda}_{n,\mu} \lambda_{n,\mu} = 1 . \quad (2b)$$

We also considered its tree Symanzik improved counterpart [15]

$$S_g^{\mathrm{Sym}} = -N\beta \left[\frac{4}{3} \sum_{n,\mu} (\bar{z}_{n+\mu} z_n \lambda_{n,\mu} + \bar{z}_n z_{n+\mu} \bar{\lambda}_{n,\mu} - 2) - \frac{1}{12} \sum_{n,\mu} (\bar{z}_{n+2\mu} z_n \lambda_{n,\mu} \lambda_{n+\mu,\mu} + \bar{z}_n z_{n+2\mu} \bar{\lambda}_{n,\mu} \bar{\lambda}_{n+\mu,\mu} - 2) \right] . \quad (3)$$

Tests of rotation invariance and stability of dimensionless ratios of physical quantities showed that the above actions lead to scaling for rather small correlation lengths [4]. A comparison of measurements performed using these two actions will provide a check of universality, implying that the two actions are different regularizations of a unique quantum field theory.

Since the two actions are linear with respect to each lattice variable, it is easy to construct efficient local algorithms based on overrelaxation procedures. In our simulations we employed algorithms consisting in efficient mixtures of over-heat-bath [16] and microcanonical [17] algorithms. The detailed description of this simulation algorithm with a discussion of its dynamical features is contained in Ref. [4].

An important class of observables can be constructed by considering the local gauge-invariant composite operator

$$P_{ij}(x) = \bar{z}_i(x) z_j(x) \quad (4)$$

and its group-invariant correlation function

$$G_P(x) = \langle \mathrm{Tr}\, P(x) P(0) \rangle_{\mathrm{conn}} . \quad (5)$$

The standard correlation length ξ_w is extracted from the long-distance behavior of the zero space momentum correlation function ("wall-wall" correlation). The expected large-distance behavior, including periodic boundary condition effects, is

$$G_w(x) \simeq \frac{A_w}{2} \left[\exp\left(-\frac{x}{\xi_w}\right) + \exp\left(-\frac{L-x}{\xi_w}\right) \right] \quad \text{for} \quad \frac{L}{2} > x \gg \xi_w . \quad (6)$$

Moreover we measured the "diagonal wall-wall" correlation length ξ_d, obtained by summing on the correlations between points located on two distinct parallel lines oriented at 45° with respect to the coordinate axes, whose large distance behavior should be

$$G_d(x) \simeq \frac{A_d}{2} \left[\exp\left(-\frac{x}{\xi_d}\right) + \exp\left(-\frac{L/\sqrt{2}-x}{\xi_d}\right) \right] \quad \text{for} \quad \frac{L}{2\sqrt{2}} > x \gg \xi_d . \quad (7)$$

In practice, ξ_w, ξ_d, A_w, and A_d will be obtained by fitting the data for G_w and G_d by the functions (6) and (7), using all the values of x larger than a value $x_{\min}$ to be determined. The comparison between ξ_w and ξ_d provides a test of rotation invariance. Indeed in the scaling region, rotation invariance implies $\xi_w = \xi_d$ and $A_w = A_d$. Both ξ_w and ξ_d should reproduce in the continuum limit the inverse mass gap.

An alternative definition of the correlation length ξ_G comes from considering the second moment of the correlation function G_P. In the small momentum regime we expect the behavior

$$\widetilde{G}_P(k) \approx \frac{Z_P}{\xi_G^{-2} + k^2} , \quad (8)$$

where $\widetilde{G}_P(k)$ is the Fourier transform of $G_P(x)$. The zero component of $\widetilde{G}_P(k)$ is by definition the magnetic susceptibility χ_m. On the lattice we can use the two lowest components of $\widetilde{G}_P(k)$ to obtain the following definition of ξ_G:

$$\xi_G^2 = \frac{1}{4 \sin^2 \pi/L} \left[\frac{\widetilde{G}_P(0,0)}{\widetilde{G}_P(0,1)} - 1 \right] . \quad (9)$$

In the scaling region the ratio ξ_G/ξ_w must be a constant, scale-independent number. The large-N expansion predicts [18]

$$\frac{\xi_G}{\xi_w} \to \sqrt{\frac{2}{3}} \quad (10)$$

when $N \to \infty$, while for $N = 2$ the ratio is equal to 1 within 1% [4].

The quantity $Z_P = \chi_m \xi_G^{-2}$ is related to the renormal-

ization of the composite operator P. Its dependence on β can therefore be determined by renormalization-group considerations. One finds that

$$Z_P = c\beta^{-2}\left[1 + O\left(\frac{1}{\beta}\right)\right], \tag{11}$$

where c is a constant independent of the regularization scheme and therefore of the lattice action. In the large-N limit it turns out to be

$$c = \frac{3}{2\pi}\left[1 + \frac{8.5414}{N} + O\left(\frac{1}{N^2}\right)\right]. \tag{12}$$

In Ref. [4] the quantity $A_G = Z_P \xi_w$ was introduced. The dimensionless ratio A_w/A_G is another scheme-independent quantity, which is approximately equal to 1 in the CP^1 [or O(3) σ] model [4] and goes to zero in the large-N limit because the $\bar{z}z$ state becomes deconfined.

Rotation invariance and stability of dimensionless physical quantities characterize the scaling region. Asymptotic scaling is only needed to extract the Λ parameter of the lattice, and to check the predictions of the perturbation theory around the critical point. Of course, the requirement of scaling is weaker than that of asymptotic scaling, which is expected to be accurately testable only much closer to the critical point. On the other hand, theoretically and for all numerical experiment purposes, the scaling property is already sufficient to simulate the physics of the continuum.

Asymptotic scaling requires the ratio of any dimensional quantity to the appropriate power of the two-loop lattice scale

$$\mathrm{A}_L \propto (2\pi\beta)^{2/N} \exp(-2\pi\beta) \tag{13}$$

to go to a constant as $\beta^{-1} \to 0$ with a linear dependence on β^{-1}. Furthermore, the ratio of the Λ parameters of two different regularizations is determined by a one-loop calculation in perturbation theory. The ratio of the Λ parameters of the actions (1) and (3) is [4]

$$\frac{\Lambda_g^{\mathrm{Sym}}}{\Lambda_g} = 1.345 \exp\left(\frac{0.444}{N}\right). \tag{14}$$

In the following we will also consider a modified bare coupling extracted from the energy [19, 20]. The perturbative expansion of the internal energy is

$$E = \frac{1}{2\beta} + \frac{2N-1}{16N^2\beta^2} + O\left(\frac{1}{\beta^3}\right) \tag{15}$$

for the action S_g. Using the first term we can define

$$\beta_E = \frac{1}{2E}. \tag{16}$$

β_E may be used as an alternative bare coupling. The first two terms of the perturbative expansion of the β function are universal; therefore, the asymptotic scaling function in this new scheme is still given by Eq. (13). Substituting β with β_E in the two-loop formula (13) should be equivalent to a resummation procedure which may improve the asymptotic behavior. From the Eq. (15) we obtain the ratio of Λ_E, the Λ parameter of the β_E scheme, and Λ_g:

$$\frac{\Lambda_E}{\Lambda_g} = \exp\left[\frac{\pi(2N-1)}{4N^2}\right]. \tag{17}$$

The same can be done within the action S_g^{Sym}. In this case the perturbative expansion of the internal energy is

$$E = \frac{1}{2\beta} + \frac{0.1001N - 0.0589}{N^2\beta^2} + O\left(\frac{1}{\beta^3}\right), \tag{18}$$

and therefore we find

$$\frac{\Lambda_E^{\mathrm{Sym}}}{\Lambda_g^{\mathrm{Sym}}} = \exp\left[\frac{\pi(0.400N - 0.236)}{N^2}\right],$$
$$\frac{\Lambda_E^{\mathrm{Sym}}}{\Lambda_g} = 1.345 \exp\left[\frac{\pi(0.542N - 0.236)}{N^2}\right]. \tag{19}$$

III. SIMULATIONS

We performed Monte Carlo simulations of the CP^3 model in the two formulations (1) and (3) for several values of β corresponding to correlation lengths ξ up to 30 lattice units. A summary of the runs is presented in Table I. There the integrated autocorrelation time of the magnetic susceptibility $\tau_{\mathrm{int}}^{\chi_m}$ is also reported. In the following we will also show some data for the CP^9 model. Most of them were obtained from the simulations presented in Ref. [4], where the details of the runs were given.

The data taken on lattices of different size can be used to extract the finite-size scaling functions of the correlation length ξ_G and of the magnetic susceptibility for the CP^3 model. In the scaling region the finite-size scaling functions must be universal, that is, independent of β and of the lattice formulation, in that they should reproduce the continuum physics in a periodic box. In Figs. 1 and 2 we plot, respectively, $f_{\xi_G} = \xi_{G,L}/\xi_{G,\infty}$ and $f_{\chi_m} = \chi_{m,L}/\chi_{m,\infty}$ vs $z = L/\xi_G$ for the two actions (1) and (3). For both actions we chose a value of β corresponding to a correlation length $\xi \simeq 4$. The finite-size

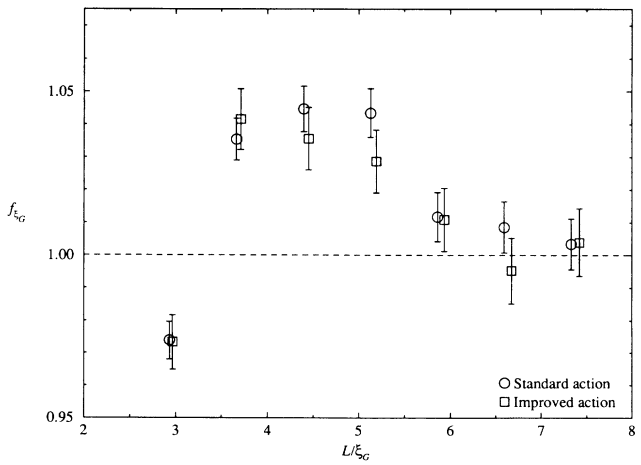

FIG. 1. Finite-size scaling of the correlation length ξ_G for the CP^3 model.

TABLE I. Summary of the simulation runs for the CP^3 model. An asterisk marks runs for the Symanzik improved action (3). We use the notation "m,γ" for a stochastic mixture of microcanonical and over-heat-bath updating with relative weigth γ (see Ref. [4]).

β	L	stat	E	ξ_G	χ_m	$\tau_{\rm int}^{\chi_m}$
0.95	12	100k m,4	0.5925(4)	3.987(14)	20.30(8)	6.1(2)
0.95	15	100k m,4	0.6005(3)	4.239(16)	22.89(8)	7.1(2)
0.95	18	100k m,4	0.6042(3)	4.277(19)	23.52(11)	7.9(3)
0.95	21	100k m,4	0.6058(2)	4.272(22)	23.64(13)	8.4(3)
0.95	24	100k m,4	0.6067(2)	4.142(23)	23.01(12)	7.3(3)
0.95	27	100k m,4	0.6070(2)	4.129(25)	22.96(11)	7.3(3)
0.95	30	100k m,4	0.6071(1)	4.108(25)	22.84(11)	7.0(2)
0.95	33	200k m,4	0.60725(8)	4.094(20)	22.81(7)	6.6(2)
1.05	60	100k m,4	0.53051(7)	7.59(8)	62.6(4)	15.8(8)
1.15	120	100k m,4	0.47341(4)	15.1(3)	189.6(2.1)	42(3)
1.20a	150	100k m,9	0.45018(4)	20.9(4)	328(4)	64(7)
1.20b	150	100k m,4	0.45011(4)	20.2(4)	317(4)	70(7)
1.25a	210	100k m,4	0.42944(3)	27.9(8)	549(10)	≈ 110
1.25b	210	100k m,9	0.42940(3)	28.3(7)	552(11)	≈ 120
0.85 *	12	100k m,4	0.6529(4)	3.936(14)	21.54(7)	6.0(2)
0.85 *	15	100k m,4	0.6578(3)	4.212(17)	24.30(10)	7.5(3)
0.85 *	18	100k m,4	0.6613(3)	4.188(20)	24.86(12)	8.3(3)
0.85 *	21	100k m,4	0.6631(2)	4.160(21)	24.82(13)	8.2(3)
0.85 *	24	100k m,4	0.6638(2)	4.088(22)	24.54(12)	8.2(3)
0.85 *	27	100k m,4	0.6640(2)	4.025(25)	24.21(12)	7.6(3)
0.85 *	30	100k m,4	0.6639(2)	4.060(27)	24.35(12)	7.7(3)
0.85 *	36	100k m,1	0.6641(2)	4.044(32)	24.28(12)	6.9(2)
0.95 *	60	100k m,4	0.57665(8)	7.36(8)	63.8(5)	16.6(9)
1.00 *	81	100k m,5	0.54199(6)	10.14(13)	106.4(1.0)	26(2)
1.05 *	120	60k m,4	0.51178(6)	13.5(3)	175(3)	40(4)
1.07 *	120	160k m,4	0.50081(4)	15.4(2)	215(2)	49(4)
1.12 *a	150	160k m,4	0.47555(3)	21.2(4)	360(8)	93(9)
1.12 *b	150	140k m,9	0.47550(4)	21.0(4)	361(5)	95(10)

TABLE II. Values and ratios of different definitions of correlation length, and correlation function coefficient for the CP^3 model.

β	L	ξ_G	ξ_w	ξ_G/ξ_w	ξ_d/ξ_w	A_w/A_G
0.95	33	4.094(20)	4.151(21)	0.985(4)	0.999(5)	0.950(13)
1.05	60	7.59(8)	7.66(14)	0.991(10)	1.014(15)	0.97(4)
1.15	120	15.1(3)	15.4(4)	0.980(16)	0.980(20)	0.93(5)
1.20	150	20.5(3)	20.7(5)	0.992(13)	0.992(17)	0.98(4)
1.25	210	28.1(5)	28.9(1.2)	0.973(21)	0.98(5)	0.91(7)
0.85 *	30	4.06(3)	4.14(4)	0.982(6)	0.998(8)	0.936(19)
0.85 *	36	4.04(3)	4.12(3)	0.982(6)	0.984(10)	0.935(21)
0.95 *	60	7.36(9)	7.46(10)	0.987(11)	0.991(14)	0.95(3)
1.00 *	81	10.14(14)	10.30(20)	0.984(12)	0.98(2)	0.95(4)
1.05 *	120	13.5(4)	13.6(5)	0.992(21)	0.98(3)	0.97(7)
1.12 *	150	21.1(3)	21.4(6)	0.983(12)	1.01(2)	0.95(4)

TABLE III. Some results for the CP^9 model.

β	ξ_G	ξ_G/ξ_w	$\beta^2 Z_P$	M_G/Λ_g	$M_G/\Lambda_g\vert_E$
0.7	2.35(3)	0.971(6)	0.905(20)	25.73(33)	20.57(27)
0.75	3.31(4)	...	0.860(20)	24.63(31)	20.46(26)
0.8	4.67(3)	0.956(6)	0.830(8)	23.65(14)	20.30(13)
0.85	6.44(6)	0.962(10)	0.823(12)	23.18(22)	20.34(19)
0.9	8.83(8)	0.973(9)	0.816(11)	22.88(21)	20.42(19)
0.7*	3.78(2)	0.968(6)	0.795(7)	22.53(11)	19.90(9)
0.75*	5.19(3)	0.974(6)	0.787(7)	22.18(13)	19.94(12)

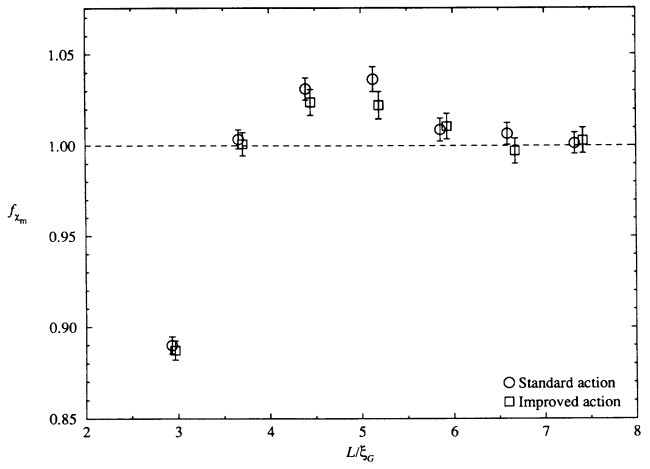

FIG. 2. Finite-size scaling of the magnetic susceptibility χ_m for the CP^3 model.

scaling functions were obtained by approximating infinite lattice quantities with the corresponding values measured on the largest lattice available. The universality with respect to the lattice action is fully satisfied. From Figs. 1 and 2 we also learn that $z \simeq 7$ is a safe value where the finite-size effects are smaller than 1%. The finite-size scaling functions for the CP^9 model were shown in Ref. [4].

Regarding the CP^3 model, the data for the different definitions of correlation length, for the correlation function coefficient A_w, and the ratio A_w/A_G are reported in Table II. The fits to G_w and G_d were performed choosing $x_{\min} \approx 2\xi_w$; fits using a larger $x_{\min}$ gave consistent results. The ratios of these different definitions were analyzed by using the jackknife method. The models defined by S_g and $S_g^{\rm Sym}$ enjoy rotation invariance and stability of dimensionless physical quantities for all values of the correlation length considered. The correlation lengths ξ_G and the ratios ξ_G/ξ_w for the CP^9 model are reported in Table III. By fitting with a constant the data of the above dimensionless ratios, we obtained the results in Table IV.

ξ_w should reproduce in the continuum limit the inverse mass of the lowest positive-parity state belonging to the adjoint representation. We also looked for other states, either excited states in the adjoint positive-parity channel, or states in the other channels, the adjoint odd channel, the singlet even and odd channels. We did not find evidence of such states for the CP^3 and the CP^9 models.

TABLE IV. Tests of scaling by fitting dimensionless ratio data with a constant.

N	S	ξ_G/ξ_w	A_w/A_G
4	S_g	0.986(3)	0.952(11)
4	$S_g^{\rm Sym}$	0.984(4)	0.944(14)
10	S_g	0.965(4)	0.870(13)
10	$S_g^{\rm Sym}$	0.971(4)	0.900(14)

TABLE V. Some results for the CP^3 model.

β	$\beta^2 Z_P$	M_G/Λ_g	$M_G/\Lambda_g\vert_E$
0.95	1.228(7)	39.1(2)	26.7(1)
1.05	1.20(2)	37.6(4)	28.5(3)
1.15	1.10(3)	33.9(6)	27.6(5)
1.20	1.10(2)	33.4(4)	27.9(4)
1.25	1.08(3)	32.7(6)	27.9(5)
0.85*	1.067(9)	33.4(2)	25.3(2)
0.95*	1.06(2)	32.7(4)	26.6(3)
1.00*	1.04(2)	31.7(4)	26.5(3)
1.05*	1.05(3)	31.7(8)	27.2(6)
1.07*	1.04(2)	31.3(4)	27.0(4)
1.12*	1.03(2)	30.6(4)	26.9(3)

Data for the constant c of Eq. (11) are reported in Tables V and III respectively for the the CP^3 and the CP^9 models. Data show scaling and the two actions give very close values. The small discrepancies can be ascribed to the nonuniversal terms of order β^{-1} in Eq. (11). We note also that the approach to scaling is slower for the action S_g.

We checked the asymptotic scaling, according to the two-loop formula $f(\beta) = (2\pi\beta)^{2/N}\exp(-2\pi\beta)$, by analyzing the quantity $M_G/\Lambda_g = [\xi_G f(\beta)]^{-1}$.

To begin with, in Fig. 3 we show data for the CP^1 model, which were taken by using the action S_g [4]. If this lattice CP^1 model belongs to the universality class of the O(3) σ model, M_G/Λ_g must tend to the asymptotic value 36.5, according to the exact result [21]. M_G/Λ_g appears to be constant within the errors for the largest values of β. Its value (approximately 47) is far from the asymptotic one. However this is not a problem, since field theory predicts an extremely slow approach to asymptopia for quantities such as M_G/Λ_g. In that region of β, corresponding to correlation lengths from about 5 to 30 lattice spacings, the β function is well approximated by the two loop formula (indeed M_G/Λ_g is constant within errors of $\sim 3\%$) but its integral does not (the discrepancy

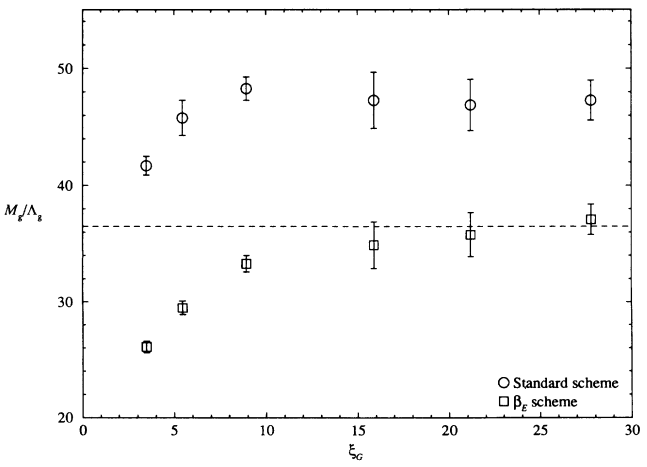

FIG. 3. Asymptotic scaling test for ξ_G in the CP^1 model.

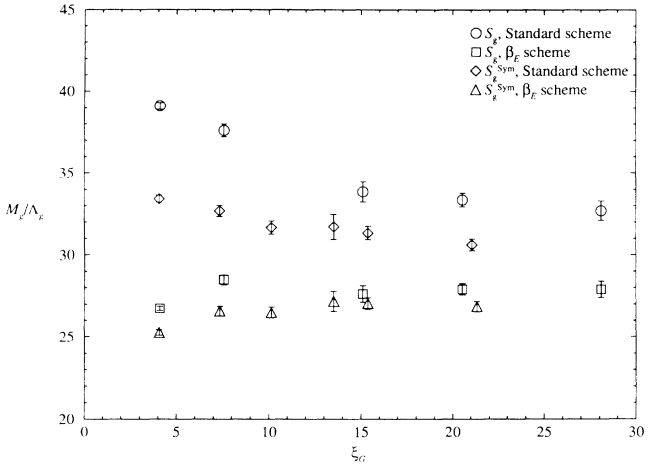

FIG. 4. Asymptotic scaling test for ξ_G in the CP^3 model.

is about 30%). It is a sort of preasymptotic region.

The situation becomes better if we use the β_E scheme. In Fig. 3 we plot also

$$\left.\frac{M_G}{\Lambda_g}\right|_E = \frac{M_G}{\Lambda_E}\frac{\Lambda_E}{\Lambda_g} \tag{20}$$

where the ratio Λ_E/Λ_g is obtained by using Eq. (17). Now data approach the correct value, represented in Fig. 3 by the continuous line. Is it only an accident?

In Tables V and III we report data of M_G/Λ_g and $M_G/\Lambda_g|_E$ for the CP^3 and the CP^9 model. We show them respectively in Fig. 4 and Fig. 5. We use the Λ ratios given in Eqs. (14) and (17) to report all data in terms of Λ_g. Again the β_E scheme improves the asymptotic scaling test. The two β_E scheme evaluations derived from the two actions S_g and $S_g^{\rm Sym}$ show good agreement. As for the CP^1 case, their value is different from those obtained with the standard schemes.

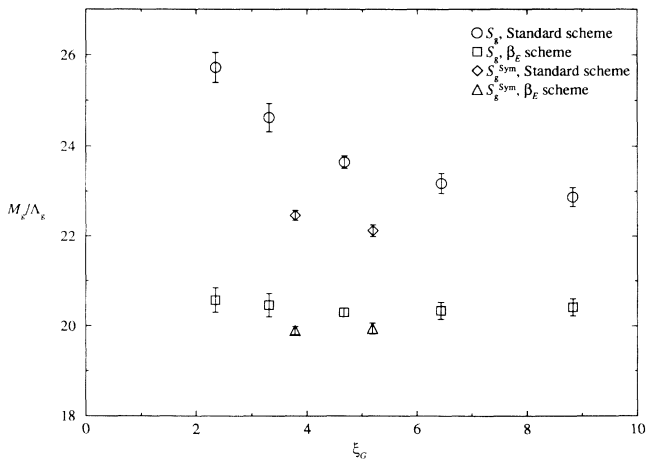

FIG. 5. Asymptotic scaling test for ξ_G in the CP^9 model.

IV. TOPOLOGICAL SUSCEPTIBILITY

A. Introduction

The topological charge density of a complex spin field z is

$$q(x) = \frac{i}{2\pi}\,\varepsilon_{\mu\nu}\,\overline{D_\mu z} D_\nu z\,. \tag{21}$$

The topological susceptibility is defined as the correlation at zero momentum of two $q(x)$ operators:

$$\chi_t = \int d^2x\,\langle q(x)\,q(0)\rangle\,. \tag{22}$$

The large-N predictions concerning the topological susceptibility are [22]

$$\chi_t \xi_w^2 = \frac{3}{4\pi N} + O(N^{-5/3})\,, \tag{23}$$

and [18]

$$\chi_t \xi_G^2 = \frac{1}{2\pi N}\left(1 - \frac{0.38}{N}\right) + O\left(\frac{1}{N^3}\right)\,. \tag{24}$$

Different methods have been proposed to calculate χ_t on the lattice. The geometrical definition uses an interpolation among discrete lattice variables to assign an integer topological charge to each lattice configuration. While for large N this definition is expected to reproduce the physical topological susceptibility, at low N χ_t^g could receive unphysical contributions from exceptional configurations, called dislocations, i.e., topological structures of the size of one lattice spacing. The dislocation contributions may either survive in the continuum limit, as it happens for some lattice formulations of the CP^1 or O(3) σ model, or push the scaling region for χ_t^g to very large β values.

Another approach relies on a definition of topological charge density by a local polynomial in the lattice variables. Local operator definitions are subject to mixing with lower and equal dimension operators and to finite renormalizations, which must be evaluated in order to extract χ_t.

A third method consists in measuring χ_t on an ensemble of configurations cooled by minimizing locally the action.

Any sensible definition of a lattice observable must show the correct scaling within each lattice formulation of the theory and universality among the determinations obtained with different lattice actions.

B. The geometrical definition

The geometrical definition of the topological charge is [12]

$$q_n^g = \frac{1}{2\pi}\,\mathrm{Im}\,\{\ln[\mathrm{Tr}\,P_{n+\mu+\nu}P_{n+\mu}P_n] + \ln[\mathrm{Tr}\,P_{n+\nu}P_{n+\mu+\nu}P_n]\}, \qquad \mu \neq \nu\,. \tag{25}$$

Introducing the quantity $\theta_{n,\mu} = \arg\{\bar{z}_n z_{n+\mu}\}$, one easily obtains

TABLE VI. Geometric and cooled topological susceptibility for the CP^9 model.

β	L	$10^4\chi_t^g$	$\chi_t^g\xi_G^2$	$10^4\chi_t^{\rm cool}$	$\chi_t^{\rm cool}\xi_G^2$
0.7	42	50.5(1.1)	0.0279(9)	...	...
0.75	60	22.6(6)	0.0248(9)	17.8(8)	0.0195(10)
0.8	60	9.9(3)	0.0216(6)	9.1(5)	0.0197(10)
0.85	72	5.1(4)	0.0213(17)	...	...
0.9	90	2.5(3)	0.0198(24)	...	...
0.7 *	42	12.3(6)	0.0179(9)	...	...
0.7 *	60	13.2(5)	0.0186(7)	12.3(4)	0.0173(7)
0.75*	81	6.5(3)	0.0176(9)	6.1(5)	0.0166(13)

$$q_n^g = \frac{1}{4\pi}\varepsilon_{\mu\nu}(\theta_{n,\mu} + \theta_{n+\mu,\nu} - \theta_{n+\nu,\mu} - \theta_{n,\nu}) . \quad (26)$$

The periodic boundary conditions make the geometrical topological charge of each lattice configuration, $Q_g = \sum_n q_n^g$, integer. The topological susceptibility should then be extracted by measuring the following expectation value

$$\chi_t^g = \frac{1}{V}\left\langle (Q_g)^2 \right\rangle . \quad (27)$$

In Table VI we report the data of χ_t^g for the CP^9 model. Using S_g the approach to scaling is slow, instead for $S_g^{\rm Sym}$ a better behavior is observed. For S_g the leading scaling-violation term must be $O(\ln\xi/\xi^2)$ when $\xi \to \infty$ [15]. Instead for the tree Symanzik improved actions the leading logarithm corrections are absent, and scale violations are $O(\xi^{-2})$ [23]. Assuming that the scaling violation term proportional to $\ln\xi/\xi^2$ is already dominant in our range of correlation lengths, we extrapolate data of $\chi_t^g\xi_G^2$ for the action S_g. In Fig. 6 we plot $\chi_t^g\xi_G^2$ vs $\ln\xi_G/\xi_G^2$. A fit gives

$$\chi_t^g\xi_G^2 = 0.0174(12) \quad b = 0.068(12) , \quad (28)$$

where b is the coefficient of the $\ln\xi_G/\xi_G^2$ term. The fitted value of $\chi_t^g\xi_G^2$ is in agreement with the value of $\chi_t^g\xi_G^2$ obtained with the action $S_g^{\rm Sym}$, which is $\chi_t^g\xi_G^2 = 0.0176(9)$ at $\xi_G = 5.19(3)$. We then conclude that for the CP^9 model χ_t^g is a good estimator of the topological susceptibility.

TABLE VII. Geometric and cooled topological susceptibility for the CP^3 model.

β	L	$10^4\chi_t^g$	$\chi_t^g\xi_G^2$	$10^4\chi_t^{\rm cool}$	$\chi_t^{\rm cool}\xi_G^2$
0.95	33	49.5(5)	0.083(1)	...	...
1.05	60	16.2(3)	0.093(3)	8.6(3)	0.050(2)
1.15	120	4.01(11)	0.091(6)	2.70(11)	0.062(3)
1.20	150	2.11(5)	0.089(3)	1.44(5)	0.061(3)
1.25	210	1.06(3)	0.084(4)	0.77(4)	0.062(4)
0.85*	36	40.5(6)	0.066(1)	...	...
0.95*	60	13.4(3)	0.072(2)	9.1(3)	0.049(2)
1.00*	81	7.0(2)	0.072(3)	5.2(2)	0.054(2)
1.05*	120	3.7(2)	0.068(4)	3.2(2)	0.058(5)
1.07*	120	2.83(7)	0.067(2)	2.37(8)	0.056(3)
1.12*	150	1.50(4)	0.067(2)	1.27(4)	0.057(2)

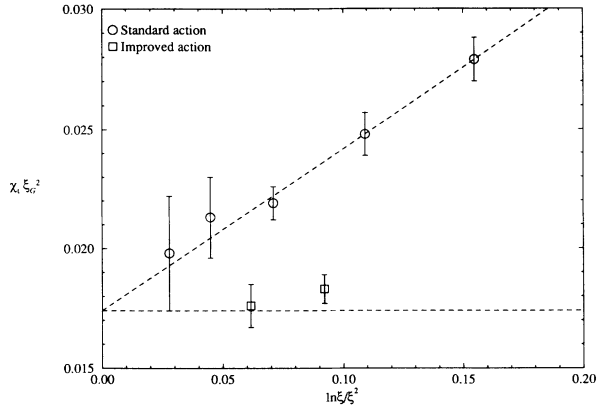

FIG. 6. Topological susceptibility vs $\ln\xi_G/\xi_G^2$ in the CP^9 model.

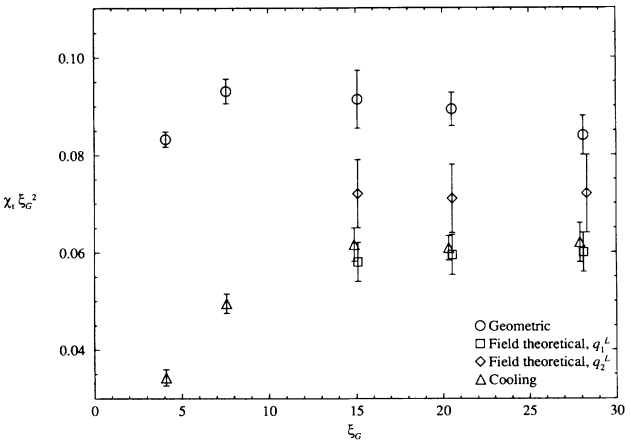

FIG. 7. Summary of the topological susceptibility determinations with the action S_g and for the CP^3 model.

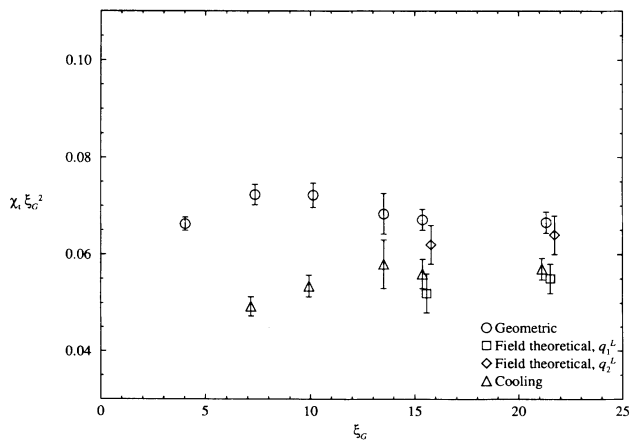

FIG. 8. Summary of the topological susceptibility determinations with the action $S_g^{\rm Sym}$ and for the CP^3 model.

The situation for the CP^3 model appears more problematic. Our data of χ_t^g for the CP^3 model are reported in Table VII and shown in Figs. 7 and 8. For both actions an apparent scaling is observed but data clearly violate universality.

C. The field-theoretical method

The field-theoretical approach relies on a definition of topological charge density by a local polynomial in the lattice variables having the correct classical continuum limit

$$q^L(x) \to a^2 q(x) + O(a^4) \tag{29}$$

(a being the lattice spacing). In order to determine χ_t, the correlation at zero momentum of two $q^L(x)$ operators χ_t^L is calculated

$$\chi_t^L = \left\langle \sum_x q^L(x) q^L(0) \right\rangle = \frac{1}{V} \left\langle \left(Q^L\right)^2 \right\rangle , \tag{30a}$$

$$Q^L = \sum_x q^L(x) . \tag{30b}$$

χ_t^L is connected to χ_t by a nontrivial relationship, since the presence of irrelevant operators of higher dimension in $q^L(x)$ induces quantum corrections. The classical continuum limit of $q^L(x)$ must be corrected including a renormalization constant $Z(\beta)$ [24]. Other contributions originate from contact terms, i.e., from the limit $x \to 0$ in Eq. (30). These contact terms appear as mixings with the trace of the energy-momentum tensor $S(x)$ and with the identity operator I, which are the only available operators with equal or lower dimension. Therefore the relationship between the lattice and the continuum topological susceptibility takes the form

$$\chi_t^L(\beta) = a^2 Z(\beta)^2 \chi_t + a^2 A(\beta) \langle S(x) \rangle_{\rm np} + P(\beta) \langle I \rangle + O(a^4) . \tag{31}$$

np denotes the nonperturbative part (i.e., the perturbative tail must be subtracted). $Z(\beta)$, $P(\beta)$, and $A(\beta)$ are ultraviolet effects, since they originate from the ultraviolet cutoff-dependent modes. They can be computed in perturbation theory as series in β^{-1}.

The field theoretical method consists in measuring $\chi_t^L(\beta)$ by a standard Monte Carlo simulation, evaluating $Z(\beta)$, $A(\beta)$, and $P(\beta)$, and using Eq. (31) to extract χ_t.

The requirement (29) does not uniquely determine the lattice operator. Different lattice versions can be found and all of them should give the same physical result for χ_t, instead the renormalization functions $Z(\beta)$, $P(\beta)$, and $A(\beta)$ are lattice operator dependent. We considered two versions of lattice topological charge density operator:

$$q_1^L(x) = -\frac{i}{2\pi} \sum_{\mu\nu} \epsilon_{\mu\nu} {\rm Tr}[P(x) \Delta_\mu^{(1)} P(x) \Delta_\nu^{(1)} P(x)] , \tag{32}$$

where $\Delta^{(1)}$ is a symmetrized version of the finite derivative,

$$\Delta_\mu^{(1)} P(x) = \tfrac{1}{2}[P(x+\mu) - P(x-\mu)] . \tag{33}$$

The second lattice operator is

$$q_2^L(x) = -\frac{i}{2\pi} \sum_{\mu\nu} \epsilon_{\mu\nu} {\rm Tr}[P(x) \Delta_\mu^{(2)} P(x) \Delta_\nu^{(2)} P(x)] , \tag{34}$$

where $\Delta^{(2)}$ is another version of finite derivative:

$$\Delta_\mu^{(2)} P(x) = \tfrac{2}{3}[P(x+\mu) - P(x-\mu)] - \tfrac{1}{12}[P(x+2\mu) - P(x-2\mu)] . \tag{35}$$

$q_2^L(x)$ is a Symanzik tree-improved version of $q_1^L(x)$.

We applied the field-theoretical method to determine the topological susceptibility of the CP^3 model.

In the following we will neglect the contribution of the mixing with $S(x)$. This assumption is supported by a perturbative argument: the perturbative series of $A(\beta)$ starts with a β^{-3} term. It will be a possible source of systematic error in our calculations.

D. The heating method

In order to estimate the renormalization functions in Eq. (31) nonperturbatively, we applied the method proposed in Ref. [25]. We start from a configuration C_0 carrying a definite topological charge Q_0 which is an approximate minimum of the lattice action (in this sense we will call it a "classical" configuration). We heat it by a local updating procedure in order to introduce short-ranged fluctuations, taking care to leave intact the background topological structure. We construct ensembles $\mathcal{C}_n^{(Q_0)}$ of many independent configurations obtained by heating the starting configuration C_0 for the same number n of updating steps, and average the topological charge over the ensembles. If $\xi \gg a$, there should exist an intermediate range of n where fluctuations of length $l \sim a$ are thermalized at the given value of β and reproduce the renormalization effects, while fluctuations at the scale $l \sim \xi$ are off equilibrium and still determined by the initial configuration. The average of $Q^L = \sum_x q^L(x)$ over the configurations in this range of n should be approximately equal to $Z(\beta)\, Q_0$.

We can also start from a constant configuration (with $Q_0 = 0$) and construct other ensembles $\mathcal{C}_n^{(0)}$ of configurations. We should find an intermediate region of n where the measure of χ_t^L gives an estimate of the mixing $P(\beta)$ with the identity operator which, being a short-ranged effect (due to the fluctuations at $l \sim a$), is expected to be independent of the physical topological background structure.

If we plot the values Q^L averaged over $\mathcal{C}_n^{(Q_0)}$ and the values of χ_t^L averaged over $\mathcal{C}_n^{(0)}$ as functions of n, we should observe plateaus in correspondence of the above-mentioned intermediate ranges. The characteristics (starting point and length) of the plateaus are determined by the phenomenon of critical slowing down. The renormalization functions are determined by short-ranged fluctuations, which we do not expect to be critically slowed down; therefore the starting point of the plateaus should be independent of β. On the other hand, the end point of the plateaus is reached when the Monte Carlo procedure changes the long-ranged modes that de-

termine the topological properties, and critical slowing down should strongly affect these modes; therefore the length of the plateaus should be β dependent. This behavior is essential for the existence of an intermediate range of n where the renormalization effects can be measured: indeed the success of the present method for estimating $Z(\beta)$ and $P(\beta)$ strongly relies on the distinction between the fluctuations at distance $l \sim a$, contributing to the renormalizations, and those at $l \sim \xi$ determining the relevant topological properties. The fluctuations at $l \sim a$ are soon thermalized, whereas the topological charge thermalization is much slower.

In order to check that heating does not change the background topological structure of the initial configuration, after a given number of heating sweeps we cool the configurations (by locally minimizing the action) and verify that the cooled configurations have topological charge equal to Q_0.

We used as an updating procedure a 20-hit Metropolis algorithm (tuned to 50% acceptance), which gives a sufficiently mild heating.

This method has been already applied to determine the topological susceptibility of the CP^1 or O(3) σ model [4, 14]. Consistency of the direct measures of $Z(\beta)$ and $P(\beta)$ with the corresponding perturbative computation has been shown in Ref. [14] within a lattice formulation of the O(3) σ model.

We construct the initial configuration carrying topological charge $Q_0 = 1$ ("lattice instanton") starting from a discretization of the continuum SU(2) instanton:

$$
\begin{aligned}
z_1(x) &= \frac{x_1 - \bar{x}_1 - i(x_2 - \bar{x}_2)}{[\rho^2 + (x_1 - \bar{x}_1)^2 + (x_2 - \bar{x}_2)^2]^{1/2}}, \\
z_2(x) &= \frac{\rho}{[\rho^2 + (x_1 - \bar{x}_1)^2 + (x_2 - \bar{x}_2)^2]^{1/2}}, \\
z_i(x) &= 0, \quad i = 3, \ldots, N, \\
\lambda_\mu(x) &= \frac{\bar{z}(x+\mu)z(x)}{|\bar{z}(x+\mu)z(x)|}.
\end{aligned}
\tag{36}
$$

The parameter ρ controls the size of the instanton, and $\bar{x}$ is its center, which we always place at the lattice center:

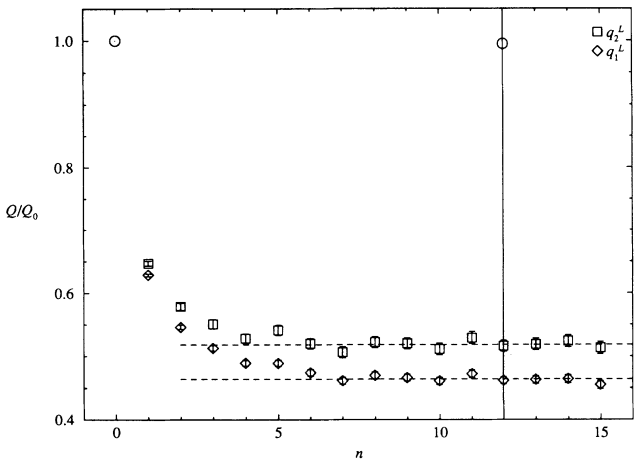

FIG. 9. Determination of the multiplicative renormalization constants Z_i^L for the tree Symanzik improved action at $\beta = 1.12$.

$\bar{x} = (L/2, L/2)$. Starting from the configuration (36), we performed a few cooling steps in order to smooth over the configuration at the lattice periodic boundary. After this procedure, we end up with a smooth configuration $C_0^{(1)}$ with topological charge $Q^L \approx 1$. The geometrical topological charge of this configuration is exactly equal to 1.

In Fig. 9 we plot $Q_1(C_n^{(1)})/Q_{0,1}$ and $Q_2(C_n^{(1)})/Q_{0,2}$, where $Q_i(C_n^{(1)})$ $(i = 1, 2)$ is the lattice topological charge $Q_i^L = \sum_x q_i^L(x)$ averaged over the ensemble $C_n^{(1)}$, $Q_{0,i}$ is the topological charge of the starting configuration measured by the operator Q_i^L. The data in Fig. 9 were taken at $\beta = 1.12$ and for the tree Symanzik improved action. We see clearly a plateau starting from $n = 7$ for both operators. For $n = 12$ we also cooled the sample of configurations finding $Q_i^L \simeq Q_{0,i}$ after a few cooling steps. This value of n is marked by a dashed line in Fig. 9. According to the above considerations, the value of Q_i^L at the plateau gives an estimate of $Z_i(\beta)$. We repeated this procedure for other values of β, and for both actions (1)

TABLE VIII. Measure of the multiplicative renormalization of χ^L, starting from an instanton of size ρ or two instantons of size ρ and distance d. Q_G is the geometrical charge of the initial configuration. The estimate of Z_i^L are taken by averaging the data in the range of n reported in the column "plateau."

β	L	Q_G	ρ	d	Stat	Plateau	$Q_{1,0}$	Z_1^L	$Q_{2,0}$	Z_2^L
1.15	48	1	10	···	1000	8–10	0.9908	0.375(7)	0.9997	0.420(12)
1.15	60	2	8	12	400	8–10	1.9165	0.375(8)	1.9912	0.417(11)
1.15	60	2	8	16	400	8–10	1.9517	0.377(7)	1.9971	0.418(10)
1.20	48	1	10	···	2000	7–10	0.9908	0.413(5)	0.9997	0.461(7)
1.20	60	2	8	20	400	7–10	1.9590	0.413(7)	1.9983	0.459(10)
1.20	48	1	10	···	1000	7–10	0.9908	0.432(6)	0.9997	0.481(10)
1.07*	48	1	10	···	1000	7–10	0.9905	0.442(6)	0.9997	0.494(9)
1.12*	48	1	10	···	1000	7–12	0.9905	0.464(5)	0.9997	0.518(8)
1.17*	48	1	10	···	500	7–12	0.9905	0.487(7)	0.9997	0.541(11)

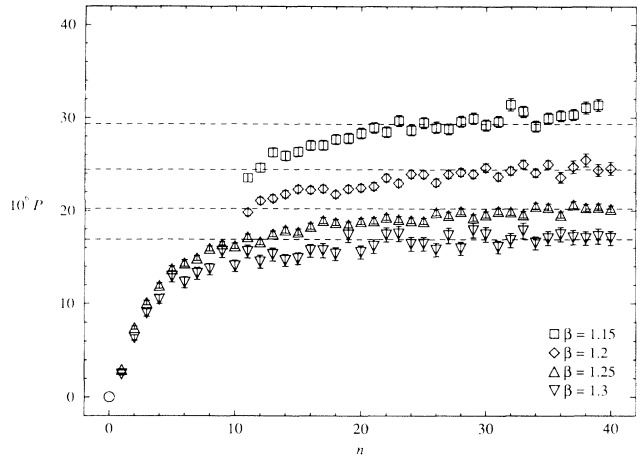

FIG. 10. Determination of the perturbative tail P of the topological susceptibility constructed with the operator q_1^L for the action S_g. Solid lines show the plateau values.

and (3). We checked also the dependence of the measure on the size of the instanton ρ (in the range of $\rho \sim \xi$), and of the value of the topological charge of the initial configuration. The behavior of $Q_i(\mathcal{C}_n^{(1)})/Q_{0,i}$ is always very similar to the case reported in Fig. 9. The results are presented in Table VIII. Configurations with topological charge two were constructed by allocating two instantons of size ρ at a distance d.

We now proceed to the analysis of the ensembles $\mathcal{C}_n^{(0)}$ of configurations obtained by heating the constant configuration $C^{(0)}$, defined by $z(x) = (0,0,0,1)$ and $\lambda_\mu(x) = 1$, for several values of β. In Figs. 10 and 11 we plot the average value of χ_t^L as a function of the number n of heating steps for the operator q_1^L and respectively for the actions (1) and (3). For every value of β we observe a plateau starting from $n \simeq 25$; the plateau is longer for higher values of β, as expected. After n_c heating sweeps (see Table IX) we cooled the sample of configurations and found vanishing Q_i^L in a few cooling steps. After the

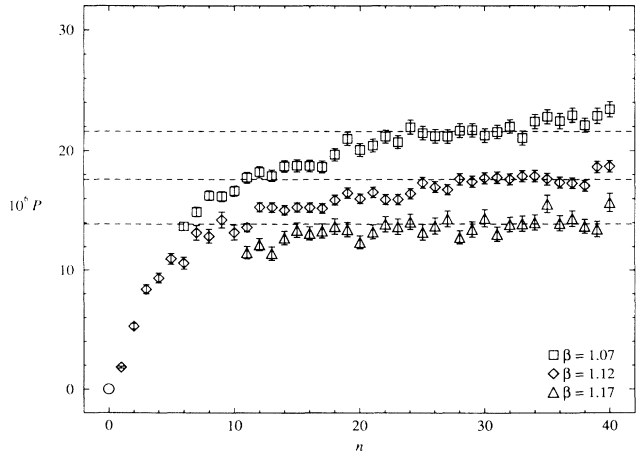

FIG. 11. Determination of the perturbative tail P of the topological susceptibility constructed with the operator q_1^L for the action S_g^{Sym}. Solid lines show the plateau values.

TABLE IX. Measure of the perturbative tail P_i of χ_i^L. Data were taken on 36×36 lattice.

β	Stat	Plateau	n_c	$10^4 P_1$	$10^4 P_2$
1.15	5000	23–30	28	0.293(6)	0.714(14)
1.20	6000	24–40	35	0.244(4)	0.592(12)
1.25	6500	28–40	40	0.202(3)	0.491(9)
1.30	1000	22–40	40	0.170(7)	0.42(2)
1.07 *	3000	24–33	28	0.215(6)	0.508(13)
1.12 *	3000	25–38	40	0.176(6)	0.414(10)
1.17 *	1000	22–40	40	0.140(6)	0.33(2)

plateau, χ_t^L increases to reach the true equilibrium value. We identify the topological susceptibility measured at the plateau $\chi_{t,p}^L$ with the perturbative tail at the given value of β. Since $Z(\beta)$ and $P(\beta)$ have their origin in the fluctuations at $l \sim a$, finite-size corrections are of the order of L^{-2} and therefore negligible on our lattice. Results are reported in Table IX.

The values of $Z(\beta)$ and $P(\beta)$ obtained by this procedure can be inserted in Eq. (31) to extract the physical value of the topological susceptibility. The results are summarized in Table X and shown in Figs. 7 and 8.

All four classes of measures (2 operators × 2 actions) show scaling within the errors. The small discrepancies among them should be explained by the mixing with the trace of the energy-momentum tensor $S(x)$ in Eq. (31). Indeed the function $A(\beta)$ is operator and action dependent and should vary slowly in the relative small range of β considered. The fact that the discrepancies are small give further support to the initial assumption of neglecting the contribution of the mixing with $S(x)$ in our calculations. From it we also get an idea of the systematic error of our calculations.

E. Heating and geometrical charge

To clarify the origin of the failure of the geometrical method, we followed the behavior of the geometrical topological susceptibility χ_t^g during the heating proce-

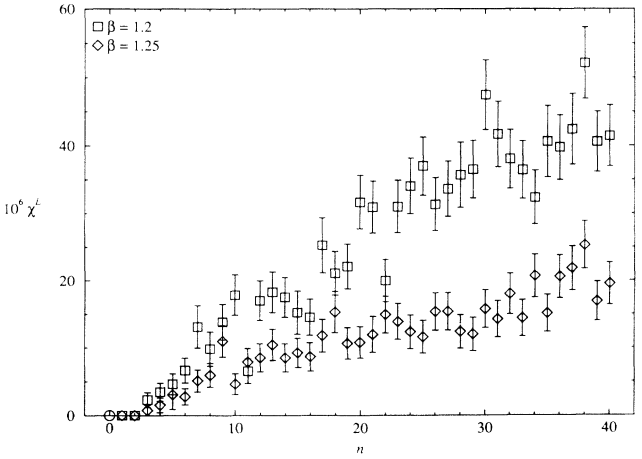

FIG. 12. Behavior of the geometrical topological susceptibility during the heating procedure using S_g.

TABLE X. Measure of χ_t by the field-theoretical method.

β	$10^4\chi_1^L$	$10^4\chi_t^{\mathrm{ft},1}$	$\chi_t^{\mathrm{ft},1}\xi_G^2$	$10^4\chi_2^L$	$10^4\chi_t^{\mathrm{ft},2}$	$\chi_t^{\mathrm{ft},2}\xi_G^2$
1.15	0.647(18)	2.52(17)	0.058(4)	1.265(36)	3.1(3)	0.071(7)
1.20	0.485(12)	1.41(8)	0.060(4)	0.952(22)	1.68(14)	0.071(5)
1.25	0.345(8)	0.76(5)	0.060(5)	0.706(15)	0.92(9)	0.072(8)
1.07*	0.646(16)	2.21(11)	0.052(4)	1.147(28)	2.62(16)	0.062(4)
1.12*	0.442(10)	1.24(6)	0.055(3)	0.800(16)	1.44(9)	0.064(4)

dure of the flat configuration. In Fig. 12 we plot $\chi_t^g(\mathcal{C}_n^{(0)})$ when heating with the action S_g at $\beta = 1.20$ and $\beta = 1.25$ (each ensemble $\mathcal{C}_n^{(0)}$ contains 1500 configurations). Again after 40 heating sweeps we cooled the configurations finding vanishing topological activity. Therefore the signals we observe in Fig. 12 are lattice artifacts, dislocation contributions. Notice that the value of χ_t^g during the heating procedure is not a negligible fraction of the corresponding results obtained at the statistical equilibrium (see Table VII). Comparing the data up to $n = 40$ for the two values of β, we do not see evidence of critical slowing down effects, which means that the modes responsible for the observed signal are the short ranged (of the size of one lattice spacing), as dislocations are supposed to be.

In Fig. 13 we plot data for $\chi_t^g(\mathcal{C}_n^{(0)})$ obtained by heating at $\beta = 1.12$ with the action S_g^{Sym}. The cooling check is again performed after 40 heating sweeps. As before we observe an apparent topological activity after a few heating sweeps, but now the signal after 40 sweeps is a smaller fraction of the total signal measured at the equilibrium condition. This should indicate that the action S_g^{Sym} is less subject to the dislocation problems.

F. Cooling method

We performed an independent measure of χ_t using the cooling method [26], which consists in measuring χ_t on an ensemble of configurations cooled by locally minimizing the action (starting from equilibrium configurations).

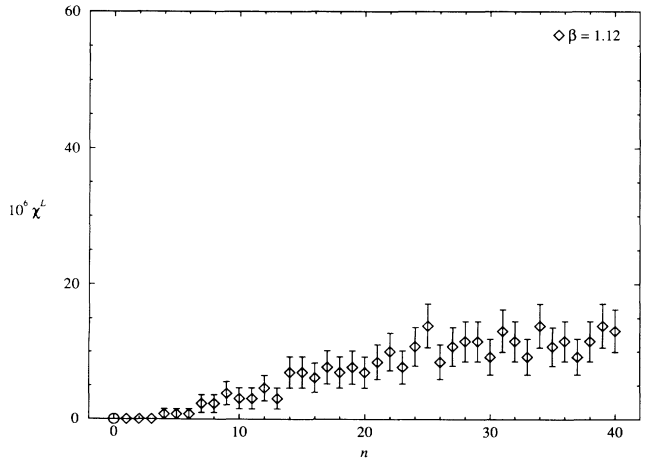

FIG. 13. Behavior of the geometrical topological susceptibility during the heating procedure using S_g^{Sym}.

The idea behind the cooling method is that local changes should not modify the topological properties of a configuration, and its topological content can be extracted from the cooled configuration, where the short-ranged fluctuations responsible of the renormalization effects, have been eliminated.

The cooling algorithm consists in assigning to each lattice variable z_n ($\lambda_{n,\mu}$) a new value z_n' ($\lambda_{n,\mu}'$) (keeping all other variables fixed) that minimizes the action.

To determine the topological charge of the cooled configurations, we used the operator $q_2^L(x)$, which turns out to be better than $q_1^L(x)$ in estimating the topological content of a smooth configuration. This can be seen by comparing the values of $Q_{0,1}$ and $Q_{0,2}$ in Table VIII. The topological susceptibility measured on cooled configurations by Eq. (30), χ_t^{cool}, is seen to gradually rise up to an extended plateau. Our averages and errors are estimated on the plateau measurements.

Table VI reports also data of some measurements of χ_t^{cool} by cooling method for the CP^9 model. These measures are quite consistent, especially those corresponding to the longest correlation lengths, with the geometrical determinations.

For the CP^3 model the results are reported in Table VII and plotted in Figs. 7 and 8. χ_t^{cool} shows scaling and the test of universality is satisfactory. Furthermore, they are consistent with the measurements obtained by the field theoretical method with the operator q_1^L.

G. Conclusions

The geometrical approach gives a good definition of lattice topological susceptibility for $N = 10$. On the other hand, we showed that $N = 4$ is not large enough to suppress the unphysical configurations contributing to χ_t^g, at least for $\xi \leq 30$. The other methods, field theoretical and cooling, give consistent measures of χ_t. We finally quote for the CP^3 model $\chi_t\xi_G^2 \simeq 0.06$ with an uncertainty of 10–20 %.

V. THE STRING TENSION

A. Wilson loops and finite-size effects

In the CP^{N-1} models it is possible to define the (Abelian) Wilson loop

$$W(\mathcal{C}) = \prod_{n,\mu\in\mathcal{C}} \lambda_{n,\mu} . \tag{37}$$

The large-N expansion predicts an exponential area law

behavior for sufficiently large Wilson loops [3],

$$W(\mathcal{C}) \sim e^{-\sigma A(\mathcal{C})-\rho P(\mathcal{C})} \quad \text{for } A(\mathcal{C}) \gg \xi^2 , \tag{38}$$

where σ is the Abelian string tension and ρ is a (renormalization-dependent) perimeter term. This implies also that the dynamical matter fields do not screen the linear potential at any distance. The large-N prediction for σ is $\sigma\xi_G^2 = \pi/N$.

Starting from the rectangular Wilson loops, we can define the Creutz ratios as

$$\chi(l,m) = \ln \frac{W(l,m-1)\,W(l-1,m)}{W(l,m)\,W(l-1,m-1)} . \tag{39}$$

The double ratio takes care of renormalization effects [constant and perimeter terms in $\ln W(l,m)$]. It is therefore easier to extract the string tension from $\chi(l,m)$.

In principle one can also define the Polyakov line and study the correlation of two such lines, thus extracting the particle-antiparticle potential. In practice the signal is so small and noisy that one can hardly extract a physically meaningful number.

In order to extract the string tension from our simulations, we should understand the behavior of the large Abelian Wilson loop of a confining theory in a 2D finite lattice with periodic boundary conditions.

To this purpose, consider a simple 2D model whose lattice gauge field propagator Δ_λ is

$$\Delta_\lambda(k) = \frac{1}{\hat{k}^2} , \quad \hat{k}_\mu^2 = 4\sin^2\frac{k_\mu}{2} . \tag{40}$$

For this model we find that a rectangular $R \times T$ Wilson loop in a $L \times L$ lattice with periodic boundary conditions has the form

$$\ln W(R,T) = -\frac{1}{2}\int \frac{d^2k}{(2\pi)^2}\frac{\sin^2(k_1R/2)}{\sin^2(k_1/2)} \times \frac{\sin^2(k_2T/2)}{\sin^2(k_2/2)}\,\hat{k}^2\Delta_\lambda(k) \tag{41}$$

where the integral must be evaluated by eliminating the zero mode. The result of the integral is

$$\ln W(R,T) = \tfrac{1}{2}RT\left(1 - \frac{RT}{L^2}\right) . \tag{42}$$

As expected the propagator defined in Eq. (40) gives rise to a linear confining potential with a string tension $\sigma = \frac{1}{2}$, but the finite-size corrections are not small. For the Creutz ratios $\eta(R) \equiv \chi(R,R)$ we obtain (in the following we will consider only Creutz ratios with equal arguments)

$$\eta(R) \equiv \chi(R,R) = \frac{1}{2}\left[1 - \left(\frac{2R-1}{L}\right)^2\right] . \tag{43}$$

From this analysis we learn that, if there are no screening effects in the CP^{N-1} models, for a sufficiently large R the behavior of the Creutz ratios $\eta(R)$ should be

$$\eta(R) \simeq \sigma\left[1 - \left(\frac{2R-1}{L}\right)^2\right] . \tag{44}$$

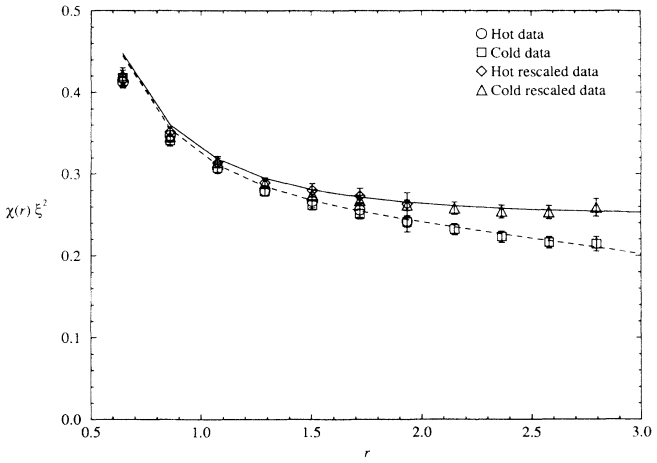

FIG. 14. Creutz ratios at $\beta = 0.8$ with the action S_g. CP^9 model. The dashed and continuous lines are respectively $\bar{\eta}^{(N)}(R)$ and $\bar{\eta}_r^{(N)}(R)$.

To compare data from different lattices it is convenient to define a rescaled Creutz ratio

$$\eta_r(R) = \eta(R)\left[1 - \left(\frac{2R-1}{L}\right)^2\right]^{-1} \simeq \sigma. \tag{45}$$

A large-N prediction for the behavior of the Creutz ratios can be obtained by substituting in Eq. (41) the following lattice regularized version of the large-N gauge field propagator:

$$\Delta_\lambda(k) = 2\pi\left(\hat{\zeta}\ln\frac{\hat{\zeta}+1}{\hat{\zeta}-1} - 2\right)^{-1} , \quad \hat{\zeta} = \sqrt{1 + \frac{1}{\xi_w^2\hat{k}^2}} . \tag{46}$$

Insertion of Eq. (46) in Eq. (41) allows us to define the quantity $\eta^{(N)}(R)$ and, applying Eq. (45), $\eta_r^{(N)}(R)$.

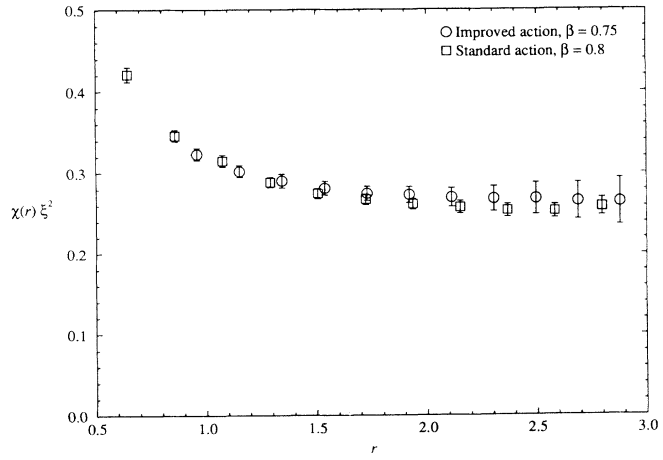

FIG. 15. Universal behavior of the rescaled Creutz ratios. CP^9 model.

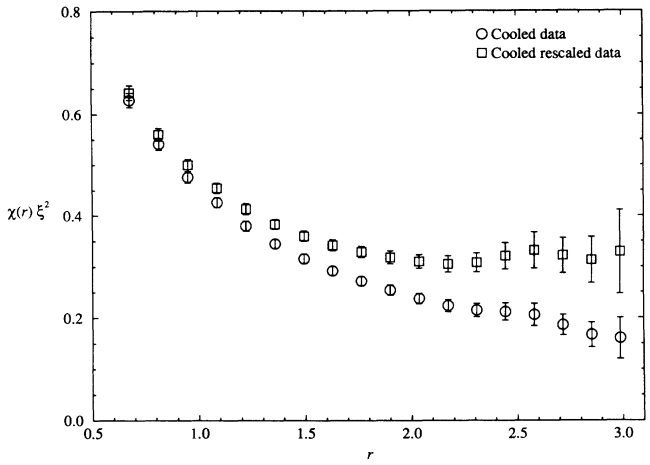

FIG. 16. Creutz ratios at $\beta = 0.95$ for the tree Symanzik improved action. CP^3 model

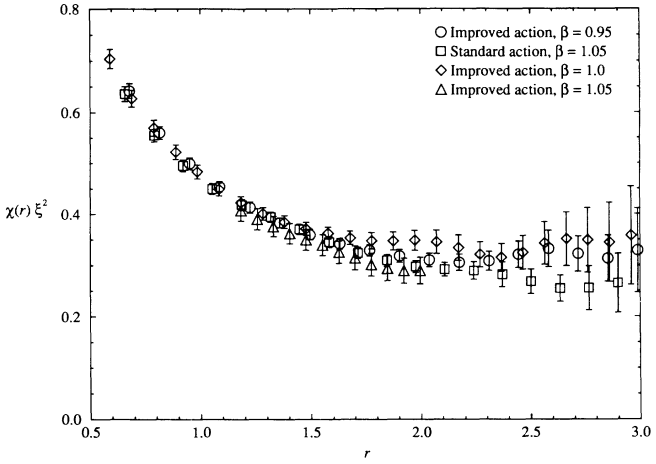

FIG. 17. Universal behavior of the rescaled Creutz ratios. CP^3 model.

B. Monte Carlo results

The gauge degrees of freedom are strongly fluctuating in the numerical simulation; therefore large Wilson loops are hard to measure. The action S_g allows us to define improved estimators for operators that are linear with respect to each $\lambda_{n,\mu}$ variable, such as the Wilson loops. Improved estimators can be obtained by replacing each $\lambda_{n,\mu}$ with its average $\lambda^{\rm imp}_{n,\mu}$ in the field of its neighbors:

$$\lambda^{\rm imp}_{n,\mu} = \frac{\int d\lambda_{n,\mu}\lambda_{n,\mu}\exp\left[2\beta N\,\mathrm{Re}\,(\bar{z}_{n+\mu}z_n\lambda_{n,\mu})\right]}{\int d\lambda_{n,\mu}\exp\left[2\beta N\,\mathrm{Re}\,(\bar{z}_{n+\mu}z_n\lambda_{n,\mu})\right]} = \frac{\bar{z}_{n+\mu}z_n}{|\bar{z}_{n+\mu}z_n|}\frac{I_1(2\beta N|\bar{z}_{n+\mu}z_n|)}{I_0(2\beta N|\bar{z}_{n+\mu}z_n|)}, \quad (47)$$

where I_0 and I_1 are modified Bessel functions.

Another way of reducing the noise is measuring the Wilson loops on cooled configurations [27]. Few cooling steps should leave intact the long-range physical quantities, such as the string tension, reducing the noise coming from the short-ranged modes. Cooling as other similar techniques, smearing and fuzzy operators, provides a sequence of approximate improved estimators. The Creutz ratios measured on cooled configurations as function of the cooling step are seen to reduce the errors and give origin to a plateau, whose length depends on the size of the involved Wilson loops. Then the cooling procedure starts to destroy the physical signal. Our averages and errors are estimated on the plateau measurements.

To begin with we present data for the CP^9 model. In Fig. 14 we show the quantities $\eta(R)\,\xi_G^2$ and $\eta_r(R)\,\xi_G^2$ vs $r = R/\xi_G$. Data were obtained by using the action S_g and at $\beta = 0.8$ on a 60×60 lattice. The improved estimators defined in Eq. (47) allow good measures up to $r \simeq 2$, for larger r the signal becomes too noisy. By using cooling we found clear signals up to $r \simeq 3$. As Fig. 14 shows, the two sets of data are in perfect agreement. Starting from $r \simeq 2$ the rescaled Creutz ratios show a clear plateau which is the evidence of the string tension. We find $\sigma\xi_G^2 = 0.25(1)$, to be compared with the large-N prediction $\sigma_N\xi_G^2 = 0.314$. This is not a surprise, in that the quantitative agreement with the $1/N$ expansion can only be reached at very large N, because of the very large coefficient in the effective expansion parameter $6\pi/N$ that can be easily extracted from a nonrelativistic Schrödinger equation analysis of the linear confining potential [2, 3].

σ_N concerns the long-range predictions of the large-N expansion. We could also test the short-distance predictions by subtracting from $\eta_r^{(N)}(R)$ the constant $a = \sigma_N - \sigma$ and comparing the new curve $\bar{\eta}_r^{(N)}(R)$ with data. In Eq. (46) as dimensional input we use the value of ξ_G, which in the large-N limit is related to ξ_w by relation (10). The results of such calculations, $\bar{\eta}^{(N)}(R)$ and $\bar{\eta}_r^{(N)}(R)$, are shown in Fig. 14 by the continuous lines.

In Fig. 15 we test the universality. Together with the above data we plot the rescaled Creutz ratios $\eta_r(R)$ measured by using the action $S_g^{\rm Sym}$ at $\beta = 0.75$ on a 60×60 lattice. These last data give $\sigma\xi_G^2 = 0.27(2)$, in agreement with the previous measure.

In Fig. 16 we show $\eta(R)$ and the corresponding rescaled ones $\eta_r(R)$ for the CP^3 model. Data were taken with the action $S_g^{\rm Sym}$ and at $\beta = 0.95$ on a 60×60 lattice and by using the cooling technique. Again starting from $r \simeq 2$ the rescaled Creutz ratios show a plateau, which gives a string tension $\sigma\xi_G^2 = 0.31(2)$.

Figure 17 shows the rescaled Creutz ratios coming from different simulations done with both actions S_g and $S_g^{\rm Sym}$, at several values of β corresponding to correlation lengths from about 7 to 15 lattice spacings, and on different lattices. The universality is fully satisfied.

In conclusion, we do not see evidence of screening effects (at least up to 3ξ) confirming the qualitative picture coming from the large-N expansion.

[1] A. D'Adda, P. Di Vecchia, and M. Lüscher, Nucl. Phys. **B146**, 63 (1978); **B152**, 125 (1979).
[2] E. Witten, Nucl. Phys. **B149**, 285 (1979).
[3] M. Campostrini and P. Rossi, Phys. Rev. D **45**, 618 (1992).
[4] M. Campostrini, P. Rossi, and E. Vicari, Phys. Rev. D **46**, 2647 (1992).
[5] K. Jensen and U. J. Wiese, Nucl. Phys. **B370**, 762

(1992).
[6] M. Hasenbusch and S. Meyer, Phys. Rev. Lett. **68**, 435 (1992).
[7] M. Hasenbusch and S. Meyer, Phys. Rev. D **45**, 4376 (1992).
[8] A. C. Irving and C. Michael, Nucl. Phys. **B371** [FS11], 521 (1992).
[9] A. C. Irving and C. Michael, Liverpool Report No. LTH 283, 1992 (unpublished).
[10] U. Wolff, Phys. Lett. B **284**, 94 (1992).
[11] N. Schultka and M. Müller-Preussker, Berlin Report No. HU Berlin-IEP 2, 1992 (unpublished).
[12] B. Berg and M. Lüscher, Nucl. Phys. **B190**, 412 (1981).
[13] M. Lüscher, Nucl. Phys. **B200** [FS4], 61 (1982).
[14] A. Di Giacomo, F. Farchioni, A. Papa, and E. Vicari, preceding paper, Phys. Rev. D **46**, 4630 (1992).
[15] K. Symanzik, in *Mathematical Problems in Theoretical Physics*, edited by R. Schrader *et al.*, Lecture Notes in Physics, Vol. 153 (Springer, Berlin, 1983).
[16] R. Petronzio and E. Vicari, Phys. Lett. B **254**, 444 (1991).
[17] M. Creutz, Phys. Rev. D **36**, 515 (1987).
[18] M. Campostrini and P. Rossi, Phys. Lett. B **272**, 305 (1991).
[19] G. Parisi, in *High Energy Physics—1980*, Proceedings of the XXth Conference, Madison, Wisconsin, 1980, edited by L. Durand and L. G. Pondrom, AIP Conf. Proc. No. 68 (AIP, New York, 1981).
[20] G. Martinelli, G. Parisi, and R. Petronzio, Phys. Lett. B **100**, 485 (1981).
[21] P. Hasenfratz, M. Maggiore, and F. Niedermayer, Phys. Lett. **45B**, 522 (1990).
[22] M. Lüscher, Phys. Lett. **78B**, 465 (1978).
[23] G. Curci, P. Menotti, and G. Paffuti, Phys. Lett. **130B**, 205 (1983).
[24] M. Campostrini, A. Di Giacomo, and H. Panagopoulos, Phys. Lett. B **212**, 206 (1988).
[25] A. Di Giacomo and E. Vicari, Phys. Lett. B **275**, 429 (1992).
[26] M. Teper, Phys. Lett. B **171**, 81 (1986); **171**, 86 (1986).
[27] M. Campostrini, A. Di Giacomo, M. Maggiore, H. Panagopoulos, and E. Vicari, Phys. Lett. B **225**, 403 (1989).